UC Irvine
UC Irvine Previously Published Works

Title

Characterization of costal cartilage and its suitability as a cell source for articular cartilage tissue engineering

Permalink

https://escholarship.org/uc/item/7t85z01g

Journal

Journal of Tissue Engineering and Regenerative Medicine, 12(5)

ISSN

1932-6254

Authors

Huwe, Le W
Brown, Wendy E
Hu, Jerry C
et al.

Publication Date

2018-05-01

DOI

10.1002/term.2630

Peer reviewed

RESEARCH ARTICLE

WILEY

Characterization of costal cartilage and its suitability as a cell source for articular cartilage tissue engineering

Le W. Huwe[1] | Wendy E. Brown[2] | Jerry C. Hu[2] | Kyriacos A. Athanasiou[2] (iD)

[1] Align Technology, San Jose, CA, USA

[2] Department of Biomedical Engineering, University of California Irvine, Irvine, CA, USA

Correspondence
Kyriacos A. Athanasiou, Department of Biomedical Engineering, University of California Irvine, 3120 Natural Sciences II, Irvine, CA 92697, USA.
Email: athens@uci.edu

Abstract

Costal cartilage is a promising donor source of chondrocytes to alleviate cell scarcity in articular cartilage tissue engineering. Limited knowledge exists, however, on costal cartilage characteristics. This study describes the characterization of costal cartilage and articular cartilage properties and compares neocartilage engineered with costal chondrocytes to native articular cartilage, all within a sheep model. Specifically, we (a) quantitatively characterized the properties of costal cartilage in comparison to patellofemoral articular cartilage, and (b) evaluated the quality of neocartilage derived from costal chondrocytes for potential use in articular cartilage regeneration. Ovine costal and articular cartilages from various topographical locations were characterized mechanically, biochemically, and histologically. Costal cartilage was stiffer in compression but softer and weaker in tension than articular cartilage. These differences were attributed to high amounts of glycosaminoglycans and mineralization and a low amount of collagen in costal cartilage. Compared to articular cartilage, costal cartilage was more densely populated with chondrocytes, rendering it an excellent chondrocyte source. In terms of tissue engineering, using the self-assembling process, costal chondrocytes formed articular cartilage-like neocartilage. Quantitatively compared via a functionality index, neocartilage achieved 55% of the medial condyle cartilage mechanical and biochemical properties. This characterization study highlighted the differences between costal and articular cartilages in native forms and demonstrated that costal cartilage is a valuable source of chondrocytes suitable for articular cartilage regeneration strategies.

KEYWORDS

alternative cell source, articular cartilage regeneration, cartilage mechanical properties, cartilage tissue engineering, costal cartilage characterization, patellofemoral cartilage

1 | INTRODUCTION

Costal cartilage, present in sternal, asternal, and floating ribs of the thoracic cage, is a valuable source of graft tissue in numerous autologous therapies. These hyaline cartilage grafts are commonly used in craniofacial surgeries such as temporomandibular joint and mandible reconstructions and rhinoplasty (e.g., cosmetic nose surgery) (Chummun, McLean, Anderson, & David, 2013; Ezzat & Azizzadeh, 2013; Karagoz et al., 2012; Xingzhou et al., 2011). The use of costal cartilage has also been expanded to tracheoplasty as stent grafts (Yazdanbakhsh et al., 2015). Recently, costal cartilage has been examined in the cartilage tissue engineering field as a potential autologous or allogeneic cell source for engineering other types of cartilages (Cho et al., 2014; Murphy, DuRaine, Reddi, Hu, & Athanasiou, 2013;

O'Sullivan et al., 2015). Auricular- and articular-like cartilages have been generated using costal chondrocytes in porcine and leporine models and have shown promising outcomes. Despite the varied and impactful uses of costal cartilage as grafts and cell sources for engineered tissues in mechanically demanding anatomical locations, the properties of costal cartilage are not yet well-understood.

Only a few studies have been performed that reveal the basic properties of costal cartilage. Costal cartilage is densely populated with chondrocytes, most of which are distributed in extracellular matrix (ECM) as single cells and some as pairs or multicell clusters (Lee, Lee, Kim, & Son, 2007; M. W. Stacey et al., 2012). Like articular cartilage, costal cartilage contains high amounts of collagen and glycosaminoglycans in the ECM (Lee et al., 2007; M. Stacey et al., 2013); however, their relative compositions have not been established. The collagen

fibers in the ECM appear to be "straw-like" in structure and run longitudinally along the rib (M. W. Stacey et al., 2012). In terms of function, costal cartilage provides structural strength and flexibility to the ribcage and protects the internal organs (Lau, Oyen, Kent, Murakami, & Torigaki, 2008). To expand our knowledge on costal cartilage tissue properties, additional studies need to be performed to examine the tissue thoroughly and quantitatively.

Understanding the characteristics of costal cartilage will help determine its potential for use as a source of chondrocytes in articular cartilage repair therapies. Articular cartilage from the patellofemoral joint is commonly affected by traumatic injury and osteoarthritis (Behery, Siston, Harris, & Flanigan, 2014), and, therefore, successful cartilage repair strategies would immensely advance the clinical treatment of the joint. Costal cartilage and articular cartilage need to be quantitatively evaluated side-by-side to enhance the understanding of these tissues, to establish a benchmark of necessary properties of engineered neocartilage based on native articular cartilage, and to evaluate the potential for costal cartilage to serve as a donor source of chondrocytes. Furthermore, topographical differences in cartilage characteristics and properties have been shown previously (Shiomi et al., 2013), motivating the examination of cartilage from various topographical locations to yield a more comprehensive representation of each cartilage type. This will additionally elucidate the degree of variation among topographical locations within the same cartilage type. A thorough, parallel, and quantitative understanding of costal cartilage and articular cartilage will make strides toward establishing a heterotopic cell source and topographical cell sourcing strategies for articular cartilage tissue engineering.

Articular cartilage tissue engineering using costal chondrocytes presents advantages over using articular chondrocytes. Current autologous, *in vivo* cartilage tissue engineering strategies use cells from nonweight bearing regions of articular cartilage on the affected joint, leading to donor site morbidity in the injured joint and further degeneration (Makris, Gomoll, Malizos, Hu, & Athanasiou, 2015). Costal cartilage's high cellularity, relative tissue abundance, and surgical accessibility make it an attractive alternative cell source. Furthermore, by using costal chondrocytes, the affected joint is spared from additional injury and donor site morbidity. The use of costal chondrocytes may make articular cartilage repair therapies more available to patients with larger cartilage injuries, more progressive degeneration, or situations in which harvesting sufficient numbers of articular chondrocytes may be a challenge currently due to limited availability of healthy articular cartilage. Previous studies in porcine and leporine models have shown successful *in vitro* expansion of costal chondrocytes and subsequent neocartilage formation without ossification (Lee et al., 2007; Murphy, DuRaine, et al., 2013; Murphy, Huey, Reimer, Hu, & Athanasiou, 2013). Costal chondrocytes are also known to produce lubricin (Murphy, DuRaine, et al., 2013). Costal cartilage's tissue characteristics, the fact that the cartilage does not fully mineralize with age, and its tissue engineering potential make it a promising autologous and heterotopic cell source for articular cartilage tissue engineering strategies.

This study aimed to characterize native costal cartilage in comparison to articular cartilage and to evaluate the prospect of using costal cartilage as a source of chondrocytes for articular cartilage tissue engineering. It was conducted in two phases. The objective of Phase 1 was to quantitatively characterize and compare the properties of ovine costal cartilage and patellofemoral cartilage mechanically, biochemically, and histologically. Specifically, two regions, the tip and mid regions of the costal cartilage were examined. Within articular cartilage, three topographical locations on each of the medial condyle (MC), lateral condyle (LC), and trochlear groove (TG) regions, as well as two locations on the patella (P) region were examined. It was hypothesized that costal cartilage and patellofemoral cartilage differ in material and biochemical properties due to differences in articulation and function, despite both being hyaline. The objectives of Phase 2 were to engineer neocartilage using costal chondrocytes and evaluate the suitability of the resulting neocartilage as a potential articular cartilage replacement by comparing its functional properties to those of native articular cartilage. It was hypothesized that costal chondrocytes would form mechanically robust neocartilage and achieve compressive properties on par with native tissue.

2 | MATERIALS AND METHODS

2.1 | Native tissue sample preparation

The ribs and stifle joints of approximately 1-year-old Rambouillet Suffolk crossbred sheep were obtained from a local abattoir (Superior Farms, Dixon, CA) within 48 hr of slaughter (n = 7). Intact ribs and joints were stored at −80 °C until testing, at which point, they were thawed at 4 °C overnight and dissected at room temperature. For costal cartilage, specimens from rib numbers 12 and 13 were dissected. All muscles, fat, and perichondrium were removed from the ribs, leaving only the cartilaginous tissue. Specimens from 2 regions of the rib, the tip region (TR) and the mid region (MR), were obtained by collecting cartilage from 2 to 7 cm away from the rib tip, respectively (Figure 1). Patellofemoral articular cartilage specimens were tested from four different regions, MC, the LC, the TG, and the P. Within these different regions, multiple topographical locations were tested: three locations on MC, three locations on LC, three locations on TG, and two locations on P (Figure 1). The specimens were tested near the centerline of the condyles, groove, and patella. Native tissue samples were portioned for histological, biochemical, and mechanical evaluations.

2.2 | Cell isolation

Costal chondrocytes were isolated from the cartilaginous portion of the floating rib specimens. To obtain costal chondrocytes, cartilage was minced into 1–2 mm^3 pieces and digested in 0.2% Type II collagenase (Worthington) in Dulbecco's modified Eagle's medium (DMEM; Gibco) with 1% penicillin/streptomycin/fungizone (PSF; BD Biosciences) and 3% fetal bovine serum (FBS; Atlanta Biologicals) for 18 hr at 37 °C. After digestion, chondrocytes were filtered through 70 μm cell strainers, resuspended in blank DMEM, and counted. Approximately 6.4 million costal chondrocytes were obtained from 1 g of rib tissue. Historically, approximately 1 million articular chondrocytes are obtained from 1 g of articular cartilage, on average.
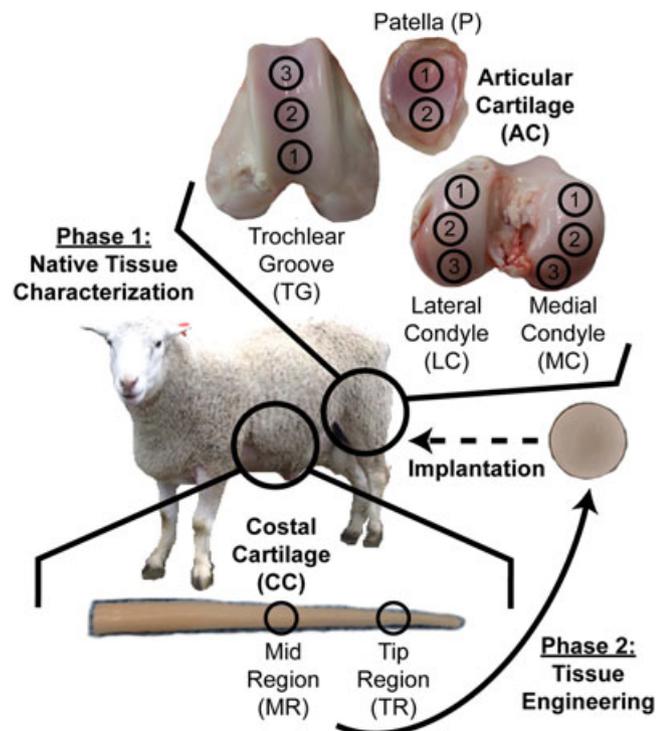
0.2% Type II collagenase in DMEM containing 1% PSF and % FBS for 1.5 hr with agitation every 20 min. Following digestion, the resulting cell solution was filtered through 70 μm cell strainers, and the cells were resuspended in blank DMEM and counted.

2.4 | Neocartilage formation and culture

Expanded, redifferentiated (P3R) costal chondrocytes were self-assembled into neocartilage constructs in nonadherent agarose wells. Agarose wells were created in a 48-well plate by inserting 5 mm-diameter, cylindrical, stainless steel posts into each well containing 1 ml of molten 2% (w/v) molecular biology grade agarose made in phosphate buffered saline for 15 min. After solidification of the agarose, the posts were removed and the wells were filled with CHG medium. Medium was exchanged three times over the course of 5 days to ensure saturation of the agarose. P3R costal chondrocytes were seeded into the wells at 2 million cells per construct in 100 μl CHG medium. Constructs were unconfined from agarose wells on Day 2, and medium exchange was performed every other day for the duration of the 28-day culture. CHG control constructs were cultured in only CHG medium. The bio-active-treated group was cultured in CHG containing 10 ng/ml TGFβ-1 throughout Days 1–28, 1.5 units/ml chondroitinase ABC (cABC) for 4 hr on Day 7, and 0.15 μg/ml lysyl oxidase-like 2 (LOXL2) with 1.6 μg/ml copper sulfate and 0.146 mg/ml hydroxylysine on Days 14–28. All evaluations took place at the end of the culture period.

2.5 | Gross morphological evaluation

The thickness of neocartilage constructs was measured from photographs using ImageJ software (National Institutes of Health). After gross pictures were taken, neocartilage constructs were portioned for histological, biochemical, and mechanical analyses.

2.6 | Histological and immunohistochemical evaluation

Native tissue and neocartilage samples were fixed in 10% neutral buffered formalin. Costal cartilage, the femoral head, and patella, except for specimens used for Von Kossa staining, were decalcified in 10% formic acid. As articular cartilage specimens were decalcified during sample processing, Von Kossa staining on these samples was not performed. All samples were further portioned into the specific regions of interest, embedded in paraffin, and sectioned along the short axis into 4 μm sections to expose the full thickness of the tissue. Sections were stained with Hematoxylin and Eosin (H&E) to show morphology, Safranin O/Fast Green to visualize glycosaminoglycans, Picrosirius Red to visualize collagen, and Von Kossa to visualize mineralization. Additionally, immunohistochemistry was performed for Collagen I (ab34710, 1:250 dilution, Abcam) and Collagen II (ab34712, 1:250 dilution, Abcam). Native sheep subchondral bone (rich in Collagen I and void of Collagen II) and articular cartilage (rich in Collagen II and void of Collagen I) were used as immunohistochemical control tissues. Anti-rabbit IgG secondary antibodies with an ABC-HRP peroxidase kit (Vector Laboratories) and DAB peroxidase (HRP) detection (Vector Laboratories) were used.

FIGURE 1 In Phase 1, articular cartilage from 11 locations across the patellofemoral joint and costal cartilage from two locations on the floating ribs was characterized histologically, biochemically, and mechanically. In Phase 2, chondrocytes isolated from costal cartilage were used to engineer neocartilage, which was compared to native articular cartilage from the medial condyle [Colour figure can be viewed at wileyonlinelibrary.com]

2.3 | Cell expansion and redifferentiation

Isolated costal chondrocytes were seeded in expansion flasks at a density of 1.4×10^4 cells per cm^2 to cover roughly 25% of flask surface area (1:4 expansion ratio) and expanded in chondrogenic medium (CHG; DMEM containing 1% PSF, 1% ITS+ premix, 1% non-essential amino acids, 10 nM dexamethasone, 40 μg/ml L-proline, 50 μg/ml ascorbate-2-phosphate, and 100 μg/ml sodium pyruvate; all from Sigma) with TFP supplementation (1 ng/ml TGFβ-1, 5 ng/ml bFGF, 10 ng/ml PDGF; all from PeproTech). Upon reaching confluence, cells were lifted from the flasks with 0.05% trypsin-EDTA (Gibco) for 5 min, and the cell layers were digested in 0.2% Type II collagenase with 1% PSF and 3% FBS for 20 min. The resulting cell solution was filtered through a 70 μm cell strainer, and the cells were resuspended in CHG medium with TFP and expanded again to reach Passage 3 (P3).

Expanded cells were cultured in 3D aggregates to revert P3 cells to the chondrocytic phenotype (P3R), as described previously (Murphy, Masters, Hu, & Athanasiou, 2013). First, petri dishes (100 mm × 20 mm) were coated with 1% (w/v) molten molecular biology grade agarose (Thermo Fisher Scientific) made in phosphate buffered saline (Sigma) to create a nonadherent environment. Then, expanded costal chondrocytes at a density of 750,000 cells/ml in CHG medium containing 10 ng/ml TGF-β1 were cultured in the petri dishes for 11 days with 1 day of shaking on an orbital shaker at 60 rpm and 10 days of static culture. Single cells were obtained from aggregates by treating the aggregates with 0.05% trypsin-EDTA for 45 min followed by

2.7 | Biochemical evaluation

Samples portioned for biochemical analysis were weighed to measure wet weight, lyophilized, and weighed again to measure dry weight. Water content of the tissues was determined from sample wet weight and dry weight before and after lyophilization. The lyophilized tissue samples were digested in 125 μg/ml papain in phosphate buffer at 60 °C for 18 hr for biochemical analyses. Sulfated GAG content was measured using the Blyscan dimethyl methylene blue assay kit (Biocolor Ltd). Collagen content was quantified by a modified colorimetric chloramine-T hydroxyproline assay using a Sircol collagen assay standard (Biocolor Ltd). A Picogreen assay (Quant-iT Picogreen dsDNA assay kit) was performed to measure the DNA content. Collagen and GAG contents were normalized to wet weight, dry weight, and DNA.

2.8 | Mechanical evaluation

Stress-relaxation compressive testing was performed on 3 mm cylindrical punches of costal cartilage, full thickness articular cartilage removed from patellofemoral surface, and engineered neocartilage. Samples were preconditioned at 5% compressive strain for 15 cycles, and then stress-relaxation tests were carried out at 10% and 20% strains. A viscoelastic model in MATLAB (MathWorks) was used to fit the data and yielded an instantaneous modulus, relaxation modulus, and coefficient of viscosity at both 10% and 20% strains (Allen & Athanasiou, 2006).

Creep indentation testing was performed on 3 mm cylindrical punches of costal cartilage and on blocks of patellofemoral osteochondral tissue, approximately 10 cm^3 by volume. Using an automated system, a 1 mm-diameter, flat, porous indenter tip was applied to the samples under a 2–3 g load to achieve 10–15% strain within the tissue. Under loading, the indenter position was measured to determine the creep compression of the tissue over time (Athanasiou et al., 1995; Mow, Gibbs, Lai, Zhu, & Athanasiou, 1989). A semianalytical, seminumerical, linear biphasic model and finite element analysis were used to obtain the aggregate modulus and shear modulus from the experimental data (Athanasiou et al., 1995). Articular cartilage thickness was immediately determined following testing of the osteochondral samples by needle indention. A 0.5-mm diameter, blunt, stainless steel needle was indented into the tissue. The displacement of the needle between two spikes in the force output (representing the needle passing from air to cartilage and cartilage to bone) was measured to determine the cartilage thickness. This indentation measurement was repeated three times in different areas over a single testing surface to yield an average value for each sample.

For uniaxial tensile testing, costal cartilage tissue, full thickness articular cartilage removed from the patellofemoral surface, and engineered neocartilage were trimmed with circular biopsy punch into dog-bone shaped specimens with a gauge length of 1.3 mm, in adherence with ASTM standards (ASTM D3039). Paper tabs were glued to the samples outside the gauge length, gripped in a TestResources mechanical tester (TestResources Inc.), and pulled at 1% of the gauge length per second until sample failure. Costal cartilage was tested axially and radially with respect to the rib orientation, and articular cartilage was tested along the axis of joint movement. The cross-sectional area of samples was measured with ImageJ and used to generate stress-stain curves. The tensile modulus was obtained by a least-squares fit of the linear region of the curve. The maximum stress yielded the ultimate tensile strength (UTS).

2.9 | Functionality index calculation

To assess the quality of neocartilage (NC) derived from costal chondrocytes, the biochemical and mechanical properties of the NC were compared to those of the articular cartilage of MC. To do so, a functionality index (FI), described previously (Elder & Athanasiou, 2009; MacBarb, Chen, Hu, & Athanasiou, 2013), was used, and the equation was modified to reflect the parameters measured in this study. The six properties that were included and equally weighted in the FI were GAG/wet weight (GAG), and collagen/wet weight (Col), 20% compressive instantaneous modulus (E^{20i}) and relaxation modulus (E^{20r}), tensile modulus (E^T), and UTS (Equation 1). The more similar the properties of NC to MC, the closer the FI value is to 1.

$$FI(NC|MC) = \frac{1}{6}\left[\begin{array}{c}\left(1-\left|\frac{GAG_{MC}-GAG_{NC}}{GAG_{MC}}\right|\right)+\left(1-\left|\frac{Col_{MC}-Col_{NC}}{Col_{MC}}\right|\right)+\left(1-\left|\frac{E^{20i}_{MC}-E^{20i}_{NC}}{E^{20i}_{MC}}\right|\right) \\ +\left(1-\left|\frac{E^{20r}_{MC}-E^{20r}_{NC}}{E^{20r}_{MC}}\right|\right)+\left(1-\left|\frac{E^T_{MC}-E^T_{NC}}{E^T_{MC}}\right|\right)+\left(1-\left|\frac{UTS_{MC}-UTS_{NC}}{UTS_{MC}}\right|\right)\end{array}\right]$$

$$(1)$$

2.10 | Statistical analysis

Statistical analyses were performed using Prism 7 software (GraphPad). In Phase 1, Student's t tests were performed comparing the TR and MR of costal cartilage for all properties except the tensile properties. As tensile properties were measured in both the axial and radial directions of each location in the costal cartilage, a one-way analysis of variance (ANOVA) comparing both directions and locations was used to analyse the tensile data. Tukey's post hoc tests were applied where appropriate. For articular cartilage samples, one-way ANOVAs followed by Tukey's post hoc tests were performed comparing the three topographical locations within the MC, LC, and TG. Student's t tests were performed comparing the two topographical locations on the P. For examination across the MC, LC, TG, and P regions, one-way ANOVAs and Tukey's post hoc tests were performed on the combined data from each region. In Phase 2, neocartilage properties were compared with the properties of the MC with Student's t tests. In figures and tables showing quantitative data, statistical significance (p value < .05) is indicated by groups marked with different symbols. All data are presented as means ± standard deviations.

3 | RESULTS

3.1 | Phase 1

3.1.1 | Gross morphology

All costal and patellofemoral cartilage appeared healthy. Costal cartilage of the floating ribs had a gradual conical shape with significantly different diameters in the TR and MR. The TR cartilage, located 2 mm from the tip, was 3.1 ± 0.2 mm in diameter. The diameter of the MR

cartilage, located 7 mm from the tip was 5.6 ± 0.0 mm. Patellofemoral cartilage was thin and translucent, and its thickness varied slightly by topography. The thicknesses of the articular cartilage of the MC1, MC2, and MC3 locations were 0.4 ± 0.1, 0.5 ± 0.1, and 0.4 ± 0.4 mm, respectively. The thicknesses of the articular cartilage of the LC1, LC2, and LC3 locations were 0.6 ± 0.3, 0.4 ± 0.1, and 0.5 ± 0.1 mm, respectively. The thicknesses of the articular cartilage of the TG1, TG2, and TG3 locations were 0.6 ± 0.1, 0.6 ± 0.1, and 0.6 ± 0.1 mm, respectively. The thicknesses of the articular cartilage of the P1 and P2 locations were 0.7 ± 0.1 and 0.7 ± 0.1 mm, respectively. No significant differences in thickness were observed among topographical locations within the different regions of the knee. However, when the overall thicknesses of each region were compared, the cartilage thickness of P was significantly greater than those of MC and LC. The average thicknesses of MC, LC, TG, and P were 0.5 ± 0.2, 0.5 ± 0.2, 0.6 ± 0.1, and 0.7 ± 0.1 mm.

3.1.2 | Histology

Visualizing costal cartilage with H&E staining showed that the tissue appeared hyaline and rich in GAG (Figure 2). Chondrocytes in costal cartilage were arranged in 3–4 cells per lacunae that were circular in shape. The TR of costal cartilage appeared more homogeneous than MR, where areas of faint hematoxylin staining were observed. Mineralization in costal cartilage, visualized by Von Kossa staining, indicated that MR contained more mineralization than TR. TR stained slightly more intensely for GAG than MR. Both regions stained for collagen. Immunohistochemistry showed Collagen II staining and faint Collagen I staining. All articular cartilage locations appeared histologically similar. Chondrocytes in articular cartilage were arranged in 1–2 cells per lacunae that were columnar in shape, and zone-specific cellular organization was evident. Articular cartilage stained for GAG and intensely for collagen, specifically Collagen II. Collagen I staining was not evident in the articular cartilage above the tidemark, only in the calcified cartilage and subchondral bone. Some differences were noted between costal cartilage and articular cartilage. Costal cartilage showed stronger staining in GAG and weaker staining in collagen than articular cartilage. Costal cartilage was more cellular than articular cartilage. Costal cartilage showed faint Collagen I staining compared to articular cartilage that did not stain. Articular cartilage stained more intensely for Collagen II than both regions of costal cartilage.

3.1.3 | Biochemical properties

The biochemical content of the native cartilage in the different topographical locations of the ribs and patellofemoral joint is shown in Table 1. Notably, the water content of TR of the costal cartilage was significantly greater than that of MR. The water content and the collagen/wet weight content of the MC1 location was significantly greater than that of MC3. LC1 contained significantly greater GAG/wet weight than LC3. The water content of TG1 was significantly greater than those of TG2 and TG3. Upon comparing costal cartilage to patellofemoral articular cartilage, it was shown that, overall, costal cartilage contained significantly greater GAG/wet weight, GAG/dry weight, GAG/DNA, and DNA/wet weight than articular cartilage (Figure 3 and Table 1). In contrast, articular cartilage contained
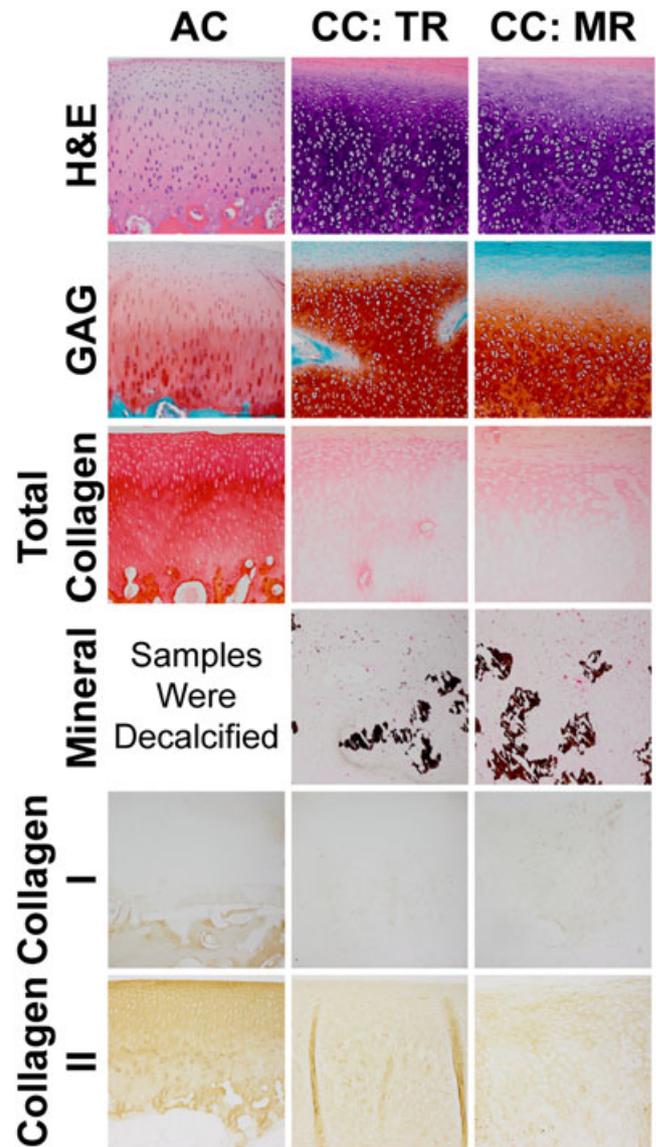

FIGURE 2 Histological and immunohistochemical evaluation of articular cartilage (AC) and the tip region (TR) and mid region (MR) of costal cartilage (CC). Both CC:TR and CC:MR stained more intensely for GAG and less intensely for total collagen and Collagen II than AC. Both CC:TR and CC:MR stained more for Collagen I than AC, but neither tissue stained strongly. CC:MR displayed more mineralization than CC:TR. GAG = glycosaminoglycan [Colour figure can be viewed at wileyonlinelibrary.com]

significantly greater collagen/wet weight and collagen/dry weight than costal cartilage (Figure 3 and Table 1). Articular cartilage was also significantly more hydrated than costal cartilage.

3.1.4 | Mechanical properties

The mechanical properties of native cartilage at the different topographical locations within regions of the ribs and the patellofemoral joint are shown in Tables 2 and 3. Notably, the costal cartilage of TR had a significantly higher 10% coefficient of viscosity and 20% relaxation modulus than MR. The tensile modulus of MC1 was significantly greater than that of MC3, and the UTS of MC1 was significantly greater than those of MC2 and MC3. The tensile modulus of MR of

TABLE 1 Biochemical properties of native costal cartilage and articular cartilage from various topographical and regional locations

Location			Water content (%)	GAG/Wet weight (%)	GAG/Dry weight (%)	GAG/DNA (µg/µg)	Collagen/Wet weight (%)	Collagen/Dry weight(%)	Collagen/DNA (µg/µg)	DNA/Wet weight (ng/µg)
Articular cartilage	Medial condyle	1	77.9 ± 0.9[A]	3.6 ± 0.2	16.3 ± 0.9	233.2 ± 108.6	18.0 ± 2.2[A]	81.7 ± 9.1	2,647.5 ± 2,374.0	0.13 ± 0.10
		2	79.2 ± 1.4[AB]	3.7 ± 0.6	17.6 ± 1.5	246.1 ± 176.9	16.0 ± 3.3[AB]	77.0 ± 15.0	1,401.3 ± 942.2	0.18 ± 0.13
		3	80.4 ± 1.2[B]	3.5 ± 0.9	17.3 ± 3.9	307.2 ± 290.6	13.3 ± 2.7[B]	67.5 ± 12.8	1,600.3 ± 1,312.2	0.22 ± 0.25
	Lateral condyle	1	77.5 ± 2.2	4.3 ± 1.1[A]	19.0 ± 3.8	331.2 ± 213.9	15.9 ± 2.2	70.8 ± 10.2	1,373.2 ± 843.0	0.14 ± 0.12
		2	79.9 ± 4.5	3.6 ± 0.4[AB]	16.9 ± 2.8	113.2 ± 55.6	15.1 ± 1.9	70.2 ± 9.3	1,325.0 ± 811.1	0.17 ± 0.14
		3	82.1 ± 5.0	2.5 ± 0.7[B]	13.6 ± 4.5	114.5 ± 91.1	15.0 ± 4.9	77.9 ± 17.4	660.8 ± 363.3	0.3 ± 0.14
	Trochlear groove	1	80.3 ± 3.7[A]	3.2 ± 1.7	15.8 ± 8.4	105.5 ± 68.8	14.2 ± 1.4	63.6 ± 16.8	553.3 ± 292.1	0.33 ± 0.24
		2	76.4 ± 2.1[B]	3.5 ± 2.8	15.3 ± 13.0	110.7 ± 127.7	16.7 ± 3.7	69.6 ± 12.3	609.3 ± 509.3	0.48 ± 0.33
		3	75.8 ± 1.0[B]	4.0 ± 1.9	16.8 ± 8.5	168.9 ± 193.5	17.4 ± 4.5	72.7 ± 19.0	972.3 ± 442.3	0.23 ± 0.16
	Patella	1	79.5 ± 2.5	3.0 ± 0.4	16.5 ± 7.2	193.4 ± 156.7	13.8 ± 5.7	73.4 ± 17.0	1,363.7 ± 1,065.3	0.14 ± 0.12
		2	82.0 ± 3.6	3.6 ± 1.2	16.8 ± 4.4	295.0 ± 241.3	14.6 ± 3.0	76.8 ± 14.9	1,195.6 ± 807.0	0.17 ± 0.11
Costal cartilage	Tip region		64.4 ± 1.9[A]	8.1 ± 2.4	22.6 ± 5.9	492.2 ± 236.3	11.6 ± 1.9	32.3 ± 5.5	1,986.1 ± 2,104.2	0.63 ± 0.02[A]
	Mid region		59.9 ± 4.8[B]	7.2 ± 1.6	22.6 ± 5.9	775.7 ± 433.0	10.8 ± 6.4	28.9 ± 19.9	776.8 ± 325.3	0.58 ± 0.05[B]

Note. Data are presented in mean ± SD.

the costal cartilage in the radial direction was greater than that of TR in the axial direction.

Upon comparing costal cartilage to patellofemoral articular cartilage, it was shown that overall, the 10% instantaneous modulus, 10% relaxation modulus, 20% instantaneous modulus, 20% relaxation modulus, aggregate modulus, and shear modulus of the costal cartilage were significantly greater than those of the patellofemoral articular cartilage (Figure 4). In contrast, the tensile modulus and UTS of the patellofemoral articular cartilage were significantly greater than those of the costal cartilage (Figure 4).

3.2 | Phase 2

Ovine costal chondrocytes proliferated quickly in monolayer expansion to Passage 3, producing 64 times the original number of cells in 19 days with cell doubling time of 3.2 days. Cell viability was maintained throughout the three-dimensional aggregate redifferentiation stage. These P3R cells formed into a cylindrical disc shaped neocartilage via the self-assembling process. The properties of the neocartilage constructs were evaluated, and the properties of the bioactive-treated neocartilage were compared to those of the articular cartilage of MC using the FI.

3.2.1 | Gross morphology

All engineered neocartilage appeared smooth, uniform, and hyaline-like. Thicknesses of the untreated and bioactive-treated engineered neocartilage constructs were 0.8 ± 0.1 and 0.7 ± 0.2 mm, respectively. Compared to native articular cartilage, the thickness of the bioactive-treated neocartilage was significantly greater than the thickness of the MC articular cartilage.

3.2.2 | Histology

By H&E staining, the bioactive-treated neocartilage appeared more cellular than the articular cartilage. Histology of the bioactive-treated neocartilage showed generally stronger GAG staining and weaker collagen staining than native articular cartilage of the MC (Figure 5). The bioactive-treated neocartilage appeared homogeneous across the depth with more intense collagen staining near the tissue perimeter. Von Kossa staining showed that no mineralization was present in the

engineered neocartilage compared to control tissue (dystrophically mineralized cardiac muscle). There was also no Collagen I staining in the bioactive-treated neocartilage. The bioactive-treated neocartilage stained comparably to native MC articular cartilage for Collagen II.

3.2.3 | Biochemical properties

The water content of the untreated and bioactive-treated neocartilage constructs were 86.2 ± 4.2% and 85.0 ± 2.9%, respectively. There was significantly more GAG per wet weight, GAG per dry weight, and GAG per DNA content in the untreated neocartilage (7.7 ± 0.5%, 48.0 ± 2.1%, and 166.0 ± 19.4 µg/µg, respectively) than the bioactive-treated neocartilage (4.8 ± 0.3%, 31.7 ± 3.3%, and 66.6 ± 7.9 µg/µg, respectively). In contrast, there was significantly more collagen per wet weight and collagen per dry weight content in the bioactive-treated neocartilage (3.3 ± 1.0% and 20.4 ± 3.6%, respectively) than the untreated neocartilage (1.5 ± 0.2% and 9.5 ± 1.2%, respectively). The collagen per DNA content of the untreated and bioactive-treated neocartilage was 32.8 ± 5.9 and 46.2 ± 14.3 µg/µg, respectively. The DNA content per wet weight of the bioactive-treated neocartilage was significantly greater than that of the untreated neocartilage, 0.71 ± 0.06 and 0.47 ± 0.02 ng/µg, respectively.

A comparison of the biochemical properties that contributed to the calculation of the FI are shown in Figure 5. When compared to the patellofemoral articular cartilage of MC, the bioactive-treated neocartilage contained significantly greater GAG/wet weight and GAG/dry weight content and significantly less collagen/wet weight, collagen/dry weight, and collagen/DNA content.

3.2.4 | Mechanical properties

The 10% relaxation modulus and 20% relaxation modulus of the control neocartilage (187.3 ± 11.2 and 275.3 ± 19.8 kPa, respectively) were significantly greater than those of the bioactive-treated neocartilage (94.9 ± 18.0 and 112.6 ± 48.2 kPa, respectively). The 10% instantaneous moduli of the control and bioactive-treated neocartilage were 247.9 ± 7.0 and 198.1 ± 66.5 kPa, respectively. The 20% instantaneous moduli of the control neocartilage and bioactive-treated constructs were 561.0 ± 36.8 and 453.8 ± 218.2 kPa, respectively. The 10% coefficients of viscosity of the control and bioactive-treated neocartilage
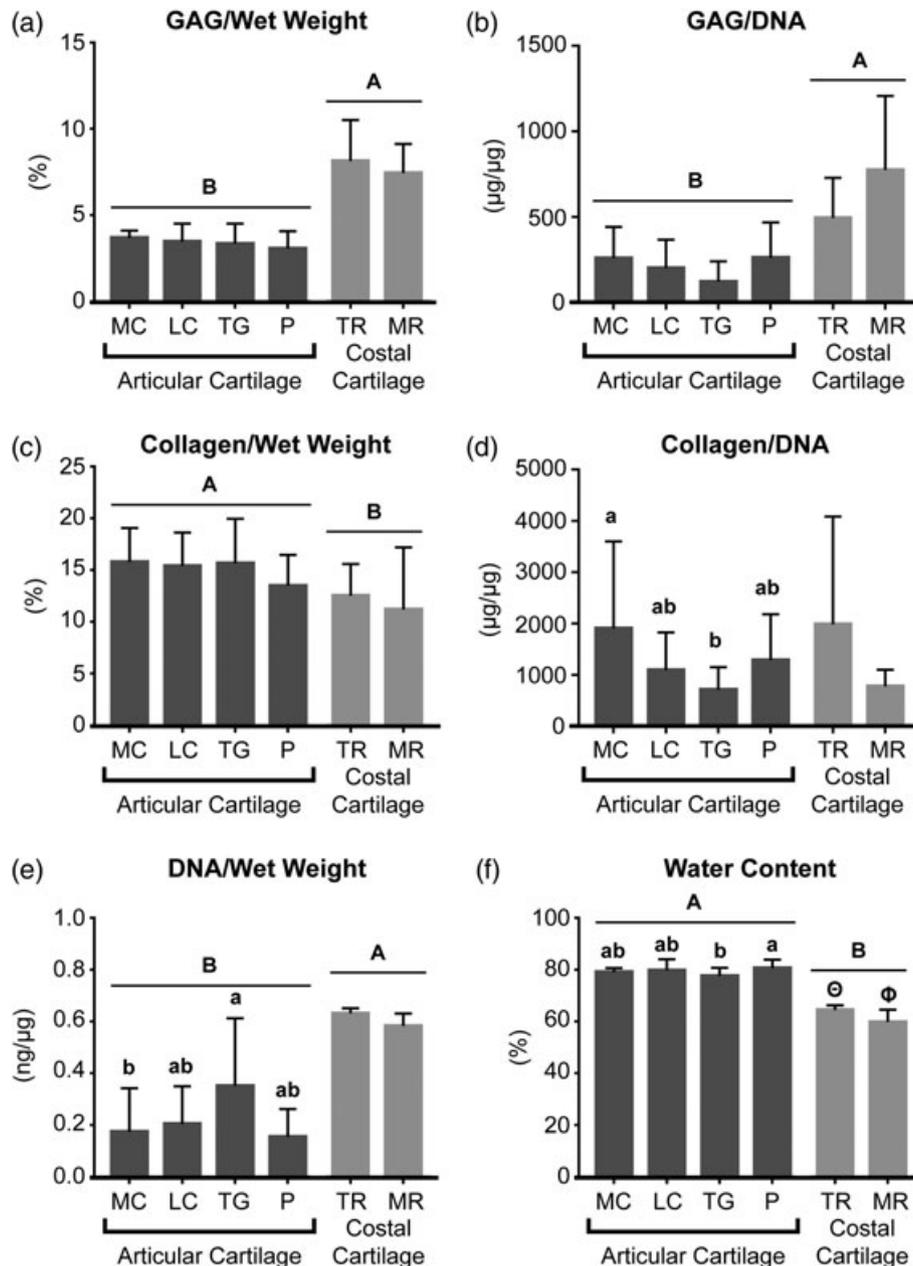
FIGURE 3 Biochemical characterization of regions of the articular cartilage (MC = medial condyle; LC = lateral condyle; TG = trochlear groove; and P = patella) and costal cartilage (TR = tip region and MR = mid region). Costal cartilage contained more GAG/wet weight (a) and GAG/DNA (b) than articular cartilage. Conversely, articular cartilage contained more collagen/wet weight (c) than costal cartilage. No differences between collagen/DNA (d) in costal cartilage and articular cartilage as a whole were observed, but regional differences were observed within the articular cartilage. Costal cartilage contained more DNA/wet weight (e) than articular cartilage, and differences were also observed within the different regions of articular cartilage. Articular cartilage was more hydrated (f) that costal cartilage and additional differences within the regions of the articular cartilage and costal cartilage were observed. Topographical biochemical data are available in Table 1. GAG = glycosaminoglycan

were 1384.3 ± 173.5 and 922.4 ± 908.5 kPa s, respectively. The 20% coefficient of viscosity of the control neocartilage (26.3 ± 9.6 MPa s) was significantly greater than that of the bioactive-treated neocartilage (3.7 ± 2.6 MPa s). The tensile modulus and the UTS of the bioactive-treated neocartilage (4.8 ± 1.5 and 1.5 ± 0.4 MPa, respectively) were significantly greater than that of the control neocartilage (1.2 ± 0.1 and 0.2 ± 0.1 MPa, respectively).

3.2.5 | Functionality index

A comparison of the mechanical properties that contributed to the calculation of the FI are shown in Figure 5. The FI, calculated to compare

the bioactive-treated neocartilage properties to articular cartilage of MC, was 0.55. This indicates that neocartilage properties reached 55% of the functional properties of native articular cartilage. The FI of untreated neocartilage was 0.10, or 10% of native articular cartilage properties.

4 | DISCUSSION

Toward assessing the utility of costal cartilage as a donor cell source for articular cartilage tissue engineering, this study was conducted in

TABLE 2 Mechanical properties from unconfined compression testing of native costal cartilage and articular cartilage from various topographical and regional locations

Testing modality			Unconfined compression					
Location			10% Inst. modulus (kPa)	10% Relax. modulus (kPa)	10% Coeffic. of viscosity (MPa s)	20% Inst. modulus (kPa)	20% Relax. modulus (kPa)	20% Coeffic. of viscosity (MPa s)
Articular cartilage	Medial condyle	1	269.9 ± 164.2	111.0 ± 34.9	3.0 ± 2.9	663.1 ± 370.8	148.6 ± 69.2	23.7 ± 18.7
		2	227.9 ± 230.5	96.9 ± 67.2	1.2 ± 2.3	414.9 ± 446.8	92.1 ± 72.3	6.9 ± 11.8
		3	233.4 ± 123.6	92.1 ± 34.4	3.1 ± 2.9	526.3 ± 259.2	96.4 ± 34.6	16.6 ± 11.6
	Lateral condyle	1	450.0 ± 286.1	157.6 ± 105.8	8.4 ± 8.3	912.7 ± 535.7	164.9 ± 101.1	36.0 ± 30.1
		2	372.7 ± 213.3	138.6 ± 66.9	5.3 ± 5.9	844.9 ± 448.2	158.9 ± 77.3	30.1 ± 25.8
		3	340.4 ± 167.9	100.9 ± 50.0	4.5 ± 3.1	789.0 ± 379.0	110.3 ± 53.8	27.0 ± 16.3
	Trochlear groove	1	279.0 ± 143.5	93.7 ± 23.8	2.9 ± 2.7	638.0 ± 291.3	108.4 ± 37.2	18.5 ± 14.0
		2	502.1 ± 355.7	157.3 ± 104.0	9.1 ± 11.6	1,078.7 ± 718.0	175.9 ± 108.1	50.4 ± 53.2
		3	444.1 ± 246.4	127.4 ± 60.8	1.7 ± 0.6	1,192.4 ± 486.4	172.6 ± 123.0	34.4 ± 34.3
	Patella	1	278.0 ± 187.2	106.7 ± 42.9	1.9 ± 2.1	637.9 ± 406.2	112.2 ± 48.4	12.5 ± 11.0
		2	361.2 ± 213.6	117.1 ± 51.6	4.3 ± 2.8	901.2 ± 603.0	127.3 ± 64.1	18.8 ± 8.4
Costal cartilage	Tip region		1,467.0 ± 897.7	803.0 ± 425.1	9.3 ± 5.6[A]	2,524.8 ± 1,007.9	1,030.9 ± 409.5[A]	52.3 ± 37.2
	Mid region		878.3 ± 584.1	550.5 ± 412.1	3.5 ± 2.4[B]	2,051.4 ± 1,113.9	997.0 ± 770.7[B]	22.5 ± 11.8

Note. Data are presented in mean ± SD.

TABLE 3 Mechanical properties from creep indentation testing and uniaxial tensile testing of native costal cartilage and articular cartilage from various topographical and regional locations

Testing modality			Creep indentation			Strain to failure	
Location			Aggregate modulus (kPa)	Shear modulus (kPa)	Permeability E-15 (m^4/N s)	Tensile modulus (MPa)	UTS (MPa)
Articular cartilage	Medial condyle	1	220.7 ± 58.2	80.4 ± 23.6	16.6 ± 14.0	18.6 ± 6.5[A]	10.1 ± 3.7[A]
		2	292.2 ± 124.1	89.6 ± 62.7	36.2 ± 25.3	13.1 ± 7.2[AB]	5.3 ± 2.9[B]
		3	182.6 ± 39.1	78.4 ± 10.5	25.9 ± 27.8	5.8 ± 1.4[B]	3.3 ± 1.0[B]
	Lateral condyle	1	299.4 ± 86.1	99.8 ± 17.2	23.7 ± 19.1	17.7 ± 8.1	13.3 ± 8.0
		2	296.8 ± 65.8	110.1 ± 29.2	46.6 ± 35.7	14.5 ± 7.6	9.9 ± 5.0
		3	283.8 ± 78.6	125.8 ± 35.4	9.2 ± 4.9	19.3 ± 4.5	11.6 ± 4.6
	Trochlear groove	1	268.5 ± 63.1	117.9 ± 25.3	12.1 ± 6.1	15.2 ± 4.6	9.0 ± 2.1
		2	302.4 ± 73.3	151.3 ± 68.1	12.8 ± 7.0	28.5 ± 16.2	17.3 ± 13.8
		3	364.0 ± 92.7	147.3 ± 37.0	27.6 ± 19.5	21.1 ± 13.0	14.0 ± 9.9
	Patella	1	296.7 ± 156.1	122.6 ± 53.1	7.2 ± 3.0	12.1 ± 4.7	7.7 ± 3.7
		2	193.0 ± 73.2	86.0 ± 33.6	7.9 ± 6.2	13.0 ± 2.7	9.0 ± 4.5
Costal cartilage	Tip region	Axial	691.0 ± 527.4	347.2 ± 152.3	7.0 ± 6.9	4.2 ± 1.6[B]	2.9 ± 1.2
		Radial				4.0 ± 1.1[AB]	2.0 ± 0.5
	Mid region	Axial	1,150.9 ± 698.8	426.7 ± 256.9	7.2 ± 5.8	7.7 ± 3.2[AB]	4.3 ± 1.5
		Radial				8.1 ± 3.7[A]	3.7 ± 2.8

Note. Data are presented in mean ± SD. UTS = ultimate tensile strength.

two phases to (a) quantitatively characterize and compare ovine costal cartilage and articular cartilage from the patellofemoral joint, and (b) assess the quality of neocartilage engineered with costal chondrocytes compared to native articular cartilage. It was hypothesized that costal cartilage and articular cartilage differ in functional properties due to differences in articulation and function. This hypothesis was confirmed, as major differences in mechanical and biochemical properties were found between costal and articular cartilages, despite both tissues being of hyaline nature. Costal cartilage was found to be 6.8-fold stiffer in compression, in terms of the 20% relaxation modulus, than articular cartilage. In contrast, articular cartilage was 146% stiffer and 171% stronger than costal cartilage in tension (Figure 4). Moreover, topographical and regional variations in properties were observed within each cartilage type. Costal cartilage showed variations in tensile properties between its mid and tip regions (Figure 4). Articular cartilage showed variations in tensile properties within its MC locations and regional variations in compressive properties within the patellofemoral joint (Table 3; Figure 4). In Phase 2, it was hypothesized that costal

chondrocytes are a suitable cell source for articular cartilage engineering because they were shown to form mechanically robust self-assembled neocartilage with compressive properties comparable to those of native articular cartilage. This hypothesis was also confirmed. Neocartilage engineered with costal chondrocytes achieved 100% of the compressive stiffness of native articular cartilage from the MC, in terms of the 20% relaxation modulus. Neocartilage tensile modulus and strength reached 37% and 23% of MC values. Costal chondrocyte derived neocartilage achieved 55% of the overall mechanical and biochemical properties of articular cartilage from MC (Figure 5), as indicated by a FI calculation. The findings of this study greatly enhance the quantitative understanding of costal cartilage in relation to articular cartilage and make strides toward establishing costal cartilage as an alternative cell source for articular cartilage tissue engineering.

The structure and physiological role of costal cartilage was found to greatly influence its mechanical properties. Compared to the tip, the MR was more mineralized, as seen by Von Kossa staining (Figure 2), and displayed significantly higher tensile properties. The
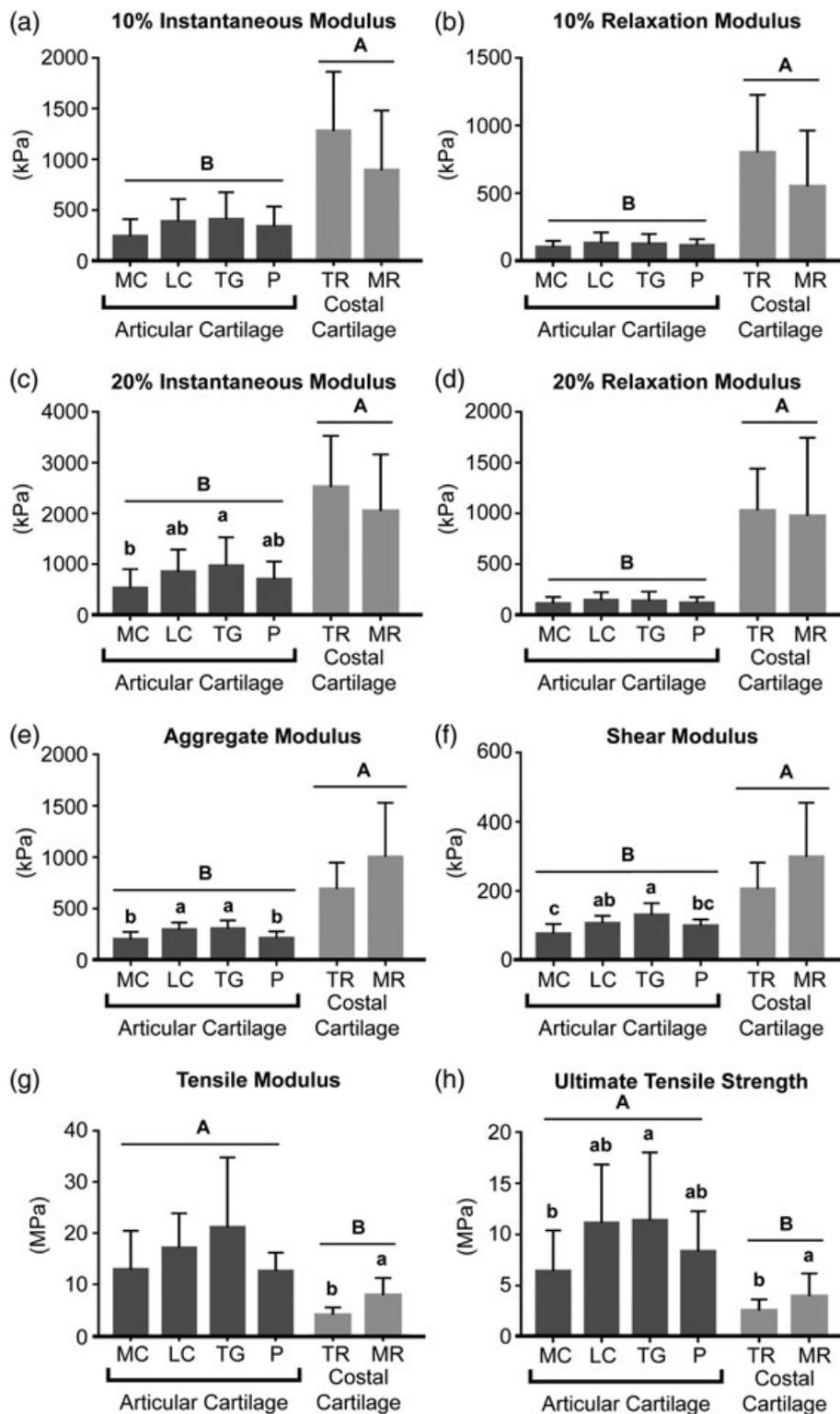
FIGURE 4 Mechanical characterization of regions of the articular cartilage (MC = medial condyle; LC = lateral condyle; TG = trochlear groove; and P = patella) and costal cartilage (TR = tip region and MR = mid region). Costal cartilage was stiffer in compression (a–f) than articular cartilage, with regional differences in 20% instantaneous modulus (c), aggregate modulus (e), and shear modulus (f) being observed within articular cartilage. Conversely, articular cartilage was stiffer and stronger than costal cartilage in tension (g and h). Differences in tensile modulus were observed across the regions of costal cartilage (g). Differences in ultimate tensile strength were observed across the regions of articular cartilage and costal cartilage (h)

distribution of mineralization was not localized to either the centerline or the periphery of the rib but spread throughout the tissue in both mid and tip regions. This agrees with the observation that mineralization is present in costal cartilage through the depth of cartilage, as shown by MRI (Forman & Kent, 2011). The MR was 93% stiffer and 55% stronger in tension than the tip (Figure 4). Moreover, it was observed that tensile properties were inversely anisotropic with respect to rib orientation between the two regions. In the TR, the
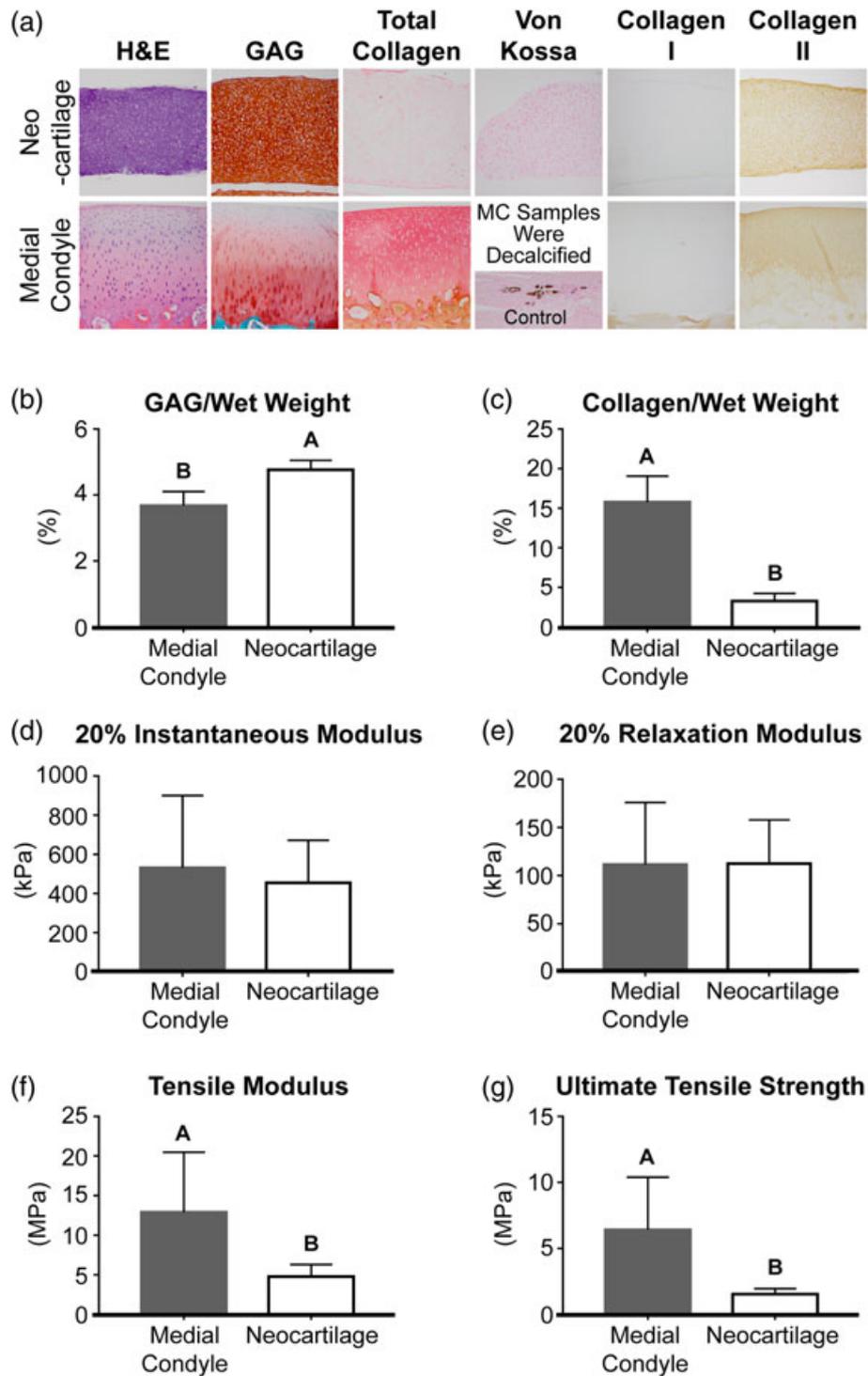
FIGURE 5 Functional comparison of engineered neocartilage compared to native articular cartilage of the medial condyle. The bioactive-treated neocartilage (neocartilage) stained more intensely for GAG than the medial condyle articular cartilage (medial condyle; a). The medial condyle showed more total collagen staining than neocartilage. Neocartilage did not stain for mineralization or Collagen I. Neocartilage Collagen II staining was comparable to the medial condyle. Neocartilage GAG/wet weight exceeds that of medial condyle (b). The 20% instantaneous modulus (d) and 20% relaxation modulus (e) of the NC are on par with MC. The collagen/wet weight content (c), tensile modulus (f), and ultimate tensile strength (g) of MC exceeds those of the NC. NC = neocartilage; MC = medial condyle; GAG = glycosaminoglycan [Colour figure can be viewed at wileyonlinelibrary.com]

tensile modulus trended higher in the axial direction than in the radial direction. However, in the MR, the tensile modulus in the radial direction trended higher than in the axial direction. The anisotropic tensile properties observed may be explained by rib and spinal movement during breathing. During normal breathing in humans, the anterior section

of the rib cage stretches circumferentially to become more elliptical during inspiration, returning to a more circular orientation during exhalation (Agostoni & Mognoni, 1966). Additionally, during breathing, the thoracic spine moves toward the posterior and upward (Leong, Lu, Luk, & Karlberg, 1998). Collagen fibers have been observed to run along the

rib axis (M. W. Stacey et al., 2012), which contribute to mechanically sustaining this motion. It is important to note, however, that rib motion during breathing, as well as the forces imposed by gravity on the rib cage, may have a different effect on quadruped animals than humans. Given the similarity in collagen and GAG contents between the mid and tip regions, the differences observed in mechanical properties are likely due to differences in matrix organization and mineralization. Although only two distinct regions were quantitatively examined in this study, histological and visual assessments suggest that costal cartilage properties vary gradually along the length of the floating rib, rather than having zone-specific or abrupt changes in properties. The present study examined the costal cartilage of the floating ribs due to its ability to serve as a minimally invasive tissue source for cartilage engineering. Additional studies should be conducted to determine the similarity of costal cartilage of floating ribs to that of true ribs. This study yielded functional properties of costal cartilage, helped elucidate its structure and function in relation to physiology, and addressed the general dearth of knowledge of this tissue.

Topographical and regional variations of functional properties observed in the ovine patellofemoral joint follow different patterns than those previously reported for the human knee. Across the ovine patellofemoral joint, the TG and LC consistently exhibited higher compressive and tensile properties than the patella and MC (Figure 4). Specifically, TG exhibited an aggregate modulus, shear modulus, tensile modulus, and UTS that were 52%, 71%, 75%, and 78% greater, respectively, than those of the MC. The LC exhibited an aggregate modulus, shear modulus, tensile modulus, and UTS that were 47%, 40%, 33%, and 74% greater, respectively, than those of the MC. These consistent patterns of mechanical properties suggest that the ovine TG may be more mechanically loaded than the MC. Notably, this pattern is different than in the human patellofemoral joint, where the MC and LC typically have the greatest compressive properties (Athanasiou, Rosenwasser, Buckwalter, Malinin, & Mow, 1991). Within the ovine patellofemoral joint, topographical differences in tensile properties were noted in the MC, but not in the LC. The tensile modulus and UTS of the MC1 location were significantly greater than MC3 by 221% and 206%, respectively (Table 3). Collagen/wet weight was also found to be significantly higher in MC1 by 35% compared to MC3 (Table 1). These patterns match those observed in lubrication studies of the bovine patellofemoral joint in which the equivalent MC1 location had a significantly lower coefficient of friction and greater compressive loading than more posterior locations (Neu, Khalafi, Komvopoulos, Schmid, & Reddi, 2007; Peng, McNary, Athanasiou, & Reddi, 2015). In contrast, tensile properties were similar across all LC locations (Table 3). Interestingly, the similarity of the coefficients of friction across anterior and posterior locations in the bovine LC (Neu et al., 2007) mirror these results. These data suggest a typical patellofemoral loading pattern amongst large quadrupeds and structure–function relationships among joint articulation, loading, and cartilage properties. Although humans and sheep have similar stifle joint anatomies, stress distributions across the joint may differ due to variations in range of motion (Proffen, McElfresh, Fleming, & Murray, 2012), resulting in differing regional patterns of cartilage properties. Sheep AC is also observed to be thinner than human AC. These and other species-dependent differences in functional properties should be considered when selecting defect locations for in vivo cartilage repair studies. As large quadrupeds, such as sheep, are commonly used and Food and Drug Administration-recognized animal models to study cartilage injury, osteoarthritis, and stifle joint diseases (Ahern, Parvizi, Boston, & Schaer, 2009; Huang, Hu, & Athanasiou, 2016; Hurtig et al., 2011), the differences between quadrupedal and bipedal joint loading and the resulting cartilage properties should be studied to inform translational pathways for cartilage repair technologies.

Costal and patellofemoral cartilages differed significantly in biochemical and mechanical properties, as well as in mineralization and cellularity. Most notably, costal cartilage compressive properties exceeded those of patellofemoral articular cartilage. Specifically, costal cartilage exhibited a greater aggregate modulus, 20% instantaneous modulus, and 20% relaxation modulus by 232%, 200%, and 6.8-fold, respectively, compared to patellofemoral cartilage (Figure 5). These differences may be explained by the structure and composition of the tissues. Costal cartilage appeared histologically heterogeneous and contained mineralized regions compared to patellofemoral cartilage, which was homogeneous and did not contain calcified regions. Additionally, costal cartilage contained 4.58-fold greater GAG/wet weight than patellofemoral cartilage (Figure 4). Both mineralization and GAG content likely contribute to costal cartilage's high compressive properties (Ebenstein, Coughlin, Chapman, Li, & Pruitt, 2009). In contrast, patellofemoral articular cartilage exhibited greater tensile properties than costal cartilage, by 146% in tensile modulus and 171% in UTS. The greater tensile properties in patellofemoral cartilage are associated with greater collagen content; patellofemoral cartilage contained 30% more collagen/wet weight than costal cartilage. It is important to note, however, that the tensile properties of patellofemoral cartilage in this study were obtained from testing a full thickness cartilage sample and are therefore slightly elevated compared to the values reported in other studies in which the superficial layer of the sample was removed (Bae et al., 2008; Charlebois, McKee, & Buschmann, 2004; Kempson, 1982). In terms of cellularity, costal cartilage contained 163% more DNA/wet weight than articular cartilage, indicating a higher cellularity in costal cartilage. The differences in cellularity were also histologically apparent (Figure 2). Within costal cartilage, DNA/wet weight content in TR was greater than MR by 8.6% (Table 1). It has been previously shown that leporine costal cartilage gave a 2.6-fold higher cell yield per the same volume of tissue as articular cartilage (Lee et al., 2007). In this study, approximately 6.4 times more cells per gram of tissue were yielded from sheep costal cartilage than articular cartilage. Therefore, using costal cartilage as an alternative donor tissue to articular cartilage for tissue engineering applications reduces the amount of donor cartilage required by eight times. The isolation of costal chondral tissue in the small amounts required may be possible through minimally invasive procedures. The high cellularity and ease of isolation compared to articular cartilage render costal cartilage, particularly from the TR that is less mineralized, an attractive alternative source of chondrocytes.

As tissue engineering and cell-based therapies rely on the cells' ability to form robust tissue to halt cartilage degeneration, the choice of cell source is critically important. Articular chondrocytes and stem cells are commonly used cell types for these cell-based therapies (Fellows, Matta, Zakany, Khan, & Mobasheri, 2016; Huang et al.,

2016). However, in an autologous cartilage repair approach, healthy articular chondrocytes have limited availability and their isolation causes donor site morbidity in already damaged areas. Stem cells require extensive *in vitro* chondrogenesis processes that are still greatly inefficient. The use of costal chondrocytes for articular cartilage tissue engineering addresses these obstacles, as they are isolated from a heterotopic source and show good expansion and redifferentiation capabilities (Murphy, DuRaine, et al., 2013; Murphy, Huey, et al., 2013). It has also been shown that during *in vitro* culture, costal chondrocytes grow faster and yield a 3-fold greater expansion up to Passage 4 than articular chondrocytes (Lee et al., 2007). The ability of these cells to undergo *in vitro* expansion further minimizes the amount of donor tissue required to obtain sufficient cell numbers for tissue engineering. In this study, using P3 and 4-fold expansion per passage, ovine costal chondrocytes expanded rapidly *in vitro* to 64 times. The restoration of a chondrogenic cellphenotype was achieved postexpansion via a 3D aggregate culture redifferentiation technique (Murphy, Masters, et al., 2013). Despite the tissue of origin being mineralized, costal chondrocytes formed scaffold-free neocartilage free of mineralization. Based on a linear scale-up of neocartilage created in this study, it is estimated that engineering neocartilage to repair a 10 cm^2 defect size would require only 0.2 g of costal cartilage. It may also be possible to expand the costal chondrocytes to a higher passage number to further minimize the volume of donor tissue required; further studies should be conducted to examine this potential. In addition to its impact on articular cartilage engineering, cell sourcing is also a major limitation to nucleus pulposus, meniscus, and TMJ disc engineering. Additional studies should be conducted to fully explore the utility of costal chondrocytes to engineer all musculoskeletal cartilages. Eliminating the need to create defects in healthy articular cartilage to isolate cells, the ability of costal chondrocytes to undergo expansion, thereby reducing the amount of required donor tissue, and their ability to form nonmineralized neocartilage make the use of costal chondrocytes a promising articular cartilage engineering strategy.

In this study, costal chondrocytes were successfully employed to form mechanically robust neocartilage with homogeneous, cartilaginous ECM consisting of GAG and Type II collagen. It has been previously shown that histology of untreated neocartilage derived from costal chondrocytes showed faint collagen and GAG staining, as well as strong Collagen II staining relative to Collagen I staining (Murphy, DuRaine, et al., 2013). In the present study, a bioactive treatment regimen, including TGF-β1, cABC, and LOXL2, further enhanced the functional properties of neocartilage engineered from costal chondrocytes. This regimen was previously examined in engineered cartilage and elicited increases in collagen production, crosslinking, and ECM compaction (Makris, MacBarb, Paschos, Hu, & Athanasiou, 2014; Murphy, Arzi, Prouty, Hu, & Athanasiou, 2015). In this study, the application of TGF-β1, cABC, and LOXL2 enhanced GAG, total collagen and Collagen II staining within the neocartilage constructs. Treatment increased collagen/wet weight by 120%; concurrently, this treatment significantly increased the neocartilage tensile modulus by 3-fold and the UTS by 6.5-fold, compared to untreated control. A FI was used for evaluating the suitability of costal chondrocyte derived neocartilage for a potential treatment in the MC, which is a common location of cartilage degeneration (Bae et al., 2010). The resulting value of 0.55

indicated that the bioactive-treated neocartilage achieved 55% of native MC articular cartilage salient mechanical and biochemical properties. Notably, the neocartilage instantaneous and relaxation moduli were 100% and 85% of the native articular cartilage from the MC (Figure 5). The neocartilage tensile modulus reached 37% of MC and the UTS reached 23%. GAG/wet weight exceeded that of the articular cartilage of the MC by 30%. Neocartilage collagen/wet weight reached 21% of MC values. Importantly, this study yielded costal chondrocyte neocartilage with compressive properties on par with native articular cartilage, highlighting the suitability of this tissue to be used for articular cartilage therapies.

5 | CONCLUSION

This study yielded a quantitative understanding of the properties of native costal cartilage and its suitability as a cell source for neocartilage engineering. Knowledge on mechanical, biochemical, and histological properties greatly enhances the understanding of costal cartilage tissue physiology and structure–function relationships. This study represents the first time costal cartilage and articular cartilage were comprehensively and quantitatively examined in a head-to-head manner. The examination revealed important differences in mechanical and biochemical properties as costal cartilage exhibited substantially higher compressive properties and lower tensile properties than articular cartilage. Additionally, topographical and regional variations found in this study are informative toward determining the best donor tissue harvest location in costal cartilage. The ovine patellofemoral topographical data significantly enhance the translational pathway for cartilage repair technologies, as it adds to the understanding of the patellofemoral joint of a commonly used preclinical model. Another innovative aspect of this work is that costal chondrocytes from an ovine source were employed to engineer neocartilage, which was then directly compared to its potential recipient site. Importantly, our evaluation concluded that costal chondrocytes constituted a suitable heterotopic cell source for articular cartilage engineering. This study confirms and expands upon previous findings that using costal chondrocytes for tissue engineering is both feasible and effective. The use of this alternative cell source is expected to greatly alleviate chondrocyte scarcity and donor site morbidity, limitations associated with current cell-based strategies, particularly for autologous therapies. Future studies should examine the long-term stability of costal chondrocyte derived neocartilage, its similarity to neocartilage engineered with articular chondrocytes, and its performance in allogeneic or autologous animal models.

CONFLICT OF INTEREST

The authors have declared that there is no conflict of interest.

ORCID

Kyriacos A. Athanasiou http://orcid.org/0000-0001-5387-8405

REFERENCES

Agostoni, E., & Mognoni, P. (1966). Deformation of the chest wall during breathing efforts. *Journal of Applied Physiology*, 21(6), 1827–1832.

Ahern, B. J., Parvizi, J., Boston, R., & Schaer, T. P. (2009). Preclinical animal models in single site cartilage defect testing: A systematic review. *Osteoarthritis and Cartilage*, 17(6), 705–713 https://doi.org/10.1016/j.joca.2008.11.008.

Allen, K. D., & Athanasiou, K. A. (2006). Viscoelastic characterization of the porcine temporomandibular joint disc under unconfined compression. *Journal of Biomechanics*, 39(2), 312–322 https://doi.org/10.1016/j.jbiomech.2004.11.012.

Athanasiou, K. A., Agarwal, A., Muffoletto, A., Dzida, F. J., Constantinides, G., & Clem, M. (1995). Biomechanical properties of hip cartilage in experimental animal models. *Clinical Orthopaedics and Related Research*, (316), 254–266.

Athanasiou, K. A., Rosenwasser, M. P., Buckwalter, J. A., Malinin, T. I., & Mow, V. C. (1991). Interspecies comparisons of in situ intrinsic mechanical properties of distal femoral cartilage. *Journal of Orthopaedic Research*, 9(3), 330–340 https://doi.org/10.1002/jor.1100090304.

Bae, W. C., Payanal, M. M., Chen, A. C., Hsieh-Bonassera, N. D., Ballard, B. L., Lotz, M. K., ... Sah, R. L. (2010). Topographic patterns of cartilage lesions in knee osteoarthritis. *Cartilage*, 1(1), 10–19 https://doi.org/10.1177/1947603509354991.

Bae, W. C., Wong, V. W., Hwang, J., Antonacci, J. M., Nugent-Derfus, G. E., Blewis, M. E., ... Sah, R. L. (2008). Wear-lines and split-lines of human patellar cartilage: relation to tensile biomechanical properties. *Osteoarthritis and Cartilage*, 16(7), 841–845 https://doi.org/10.1016/j.joca.2007.11.015.

Behery, O., Siston, R. A., Harris, J. D., & Flanigan, D. C. (2014). Treatment of cartilage defects of the knee: Expanding on the existing algorithm. *Clinical Journal of Sport Medicine*, 24(1), 21–30 https://doi.org/10.1097/JSM.0000000000000004.

Charlebois, M., McKee, M. D., & Buschmann, M. D. (2004). Nonlinear tensile properties of bovine articular cartilage and their variation with age and depth. *Journal of Biomechanical Engineering*, 126(2), 129–137.

Cho, S. A., Cha, S. R., Park, S. M., Kim, K. H., Lee, H. G., Kim, E. Y., ... Khang, G. (2014). Effects of hesperidin loaded poly(lactic-co-glycolic acid) scaffolds on growth behavior of costal cartilage cells in vitro and in vivo. *Journal of Biomaterials Science. Polymer Edition*, 25(6), 625–640 https://doi.org/10.1080/09205063.2014.888304.

Chummun, S., McLean, N. R., Anderson, P. J., & David, D. J. (2013). A long-term evaluation of 150 costochondral nasal grafts. *Journal of Plastic, Reconstructive & Aesthetic Surgery*, 66(11), 1477–1481 https://doi.org/10.1016/j.bjps.2013.07.004.

Ebenstein, D. M., Coughlin, D., Chapman, J., Li, C., & Pruitt, L. A. (2009). Nanomechanical properties of calcification, fibrous tissue, and hematoma from atherosclerotic plaques. *Journal of Biomedical Materials Research Part A*, 91(4), 1028–1037 https://doi.org/10.1002/jbm.a.32321.

Elder, B. D., & Athanasiou, K. A. (2009). Systematic assessment of growth factor treatment on biochemical and biomechanical properties of engineered articular cartilage constructs. *Osteoarthritis and Cartilage*, 17(1), 114–123 https://doi.org/10.1016/j.joca.2008.05.006.

Ezzat, W. H., & Azizzadeh, B. (2013). Costal cartilage grafting for dorsal augmentation. In A. M. Shiffman, & A. Di Giuseppe (Eds.), *Advanced aesthetic rhinoplasty: Art, science, and new clinical techniques* (pp. 479–490). Berlin, Heidelberg: Springer Berlin Heidelberg.

Fellows, C. R., Matta, C., Zakany, R., Khan, I. M., & Mobasheri, A. (2016). Adipose, bone marrow and synovial joint-derived mesenchymal stem cells for cartilage repair. *Frontiers in Genetics*, 7, 213 https://doi.org/10.3389/fgene.2016.00213.

Forman, J. L., & Kent, R. W. (2011). Modeling costal cartilage using local material properties with consideration for gross heterogeneities. *Journal of Biomechanics*, 44(5), 910–916.

Huang, B. J., Hu, J. C., & Athanasiou, K. A. (2016). Cell-based tissue engineering strategies used in the clinical repair of articular cartilage. *Biomaterials*, 98, 1–22 https://doi.org/10.1016/j.biomaterials.2016.04.018.

Hurtig, M. B., Buschmann, M. D., Fortier, L. A., Hoemann, C. D., Hunziker, E. B., Jurvelin, J. S., ... Whiteside, R. A. (2011). Preclinical studies for cartilage repair: Recommendations from the international cartilage repair society. *Cartilage*, 2(2), 137–152 https://doi.org/10.1177/1947603511401905.

Karagoz, H., Eren, F., Sever, C., Ulkur, E., Acikel, C., Celikoz, B., & Aysal, B. K. (2012). Mandibular reconstruction after hemimandibulectomy. *Journal of Craniofacial Surgery*, 23(5), 1373–1374 https://doi.org/10.1097/SCS.0b013e31825653ad.

Kempson, G. E. (1982). Relationship between the tensile properties of articular cartilage from the human knee and age. *Annals of the Rheumatic Diseases*, 41(5), 508–511.

Lau, A., Oyen, M. L., Kent, R. W., Murakami, D., & Torigaki, T. (2008). Indentation stiffness of aging human costal cartilage. *Acta Biomaterialia*, 4(1), 97–103 https://doi.org/10.1016/j.actbio.2007.06.008.

Lee, J., Lee, E., Kim, H. Y., & Son, Y. (2007). Comparison of articular cartilage with costal cartilage in initial cell yield, degree of dedifferentiation during expansion and redifferentiation capacity. *Biotechnology and Applied Biochemistry*, 48(Pt 3), 149–158 https://doi.org/10.1042/BA20060233.

Leong, J. C. Y., Lu, W. W., Luk, K. D. K., & Karlberg, E. M. (1998). Kinematics of the chest cage and spine during breathing in healthy individuals and in patients with adolescent idiopathic scoliosis. *Spine*, 24(13), 1310–1315.

MacBarb, R. F., Chen, A. L., Hu, J. C., & Athanasiou, K. A. (2013). Engineering functional anisotropy in fibrocartilage neotissues. *Biomaterials*, 34(38), 9980–9989 https://doi.org/10.1016/j.biomaterials.2013.09.026.

Makris, E. A., Gomoll, A. H., Malizos, K. N., Hu, J. C., & Athanasiou, K. A. (2015). Repair and tissue engineering techniques for articular cartilage. *Nature Reviews Rheumatology*, 11(1), 21–34 https://doi.org/10.1038/nrrheum.2014.157.

Makris, E. A., MacBarb, R. F., Paschos, N. K., Hu, J. C., & Athanasiou, K. A. (2014). Combined use of chondroitinase-ABC, TGF-beta1, and collagen crosslinking agent lysyl oxidase to engineer functional neotissues for fibrocartilage repair. *Biomaterials*, 35(25), 6787–6796 doi:S0142-9612(14)00481-5 [pii] https://doi.org/10.1016/j.biomaterials.2014.04.083.

Mow, V. C., Gibbs, M. C., Lai, W. M., Zhu, W. B., & Athanasiou, K. A. (1989). Biphasic indentation of articular cartilage—II. A numerical algorithm and an experimental study. *Journal of Biomechanics*, 22(8–9), 853–861.

Murphy, M. K., Arzi, B., Prouty, S. M., Hu, J. C., & Athanasiou, K. A. (2015). Neocartilage integration in temporomandibular joint discs: Physical and enzymatic methods. *J R Soc Interface*, 12(103). https://doi.org/10.1098/rsif.2014.1075.

Murphy, M. K., DuRaine, G. D., Reddi, A., Hu, J. C., & Athanasiou, K. A. (2013). Inducing articular cartilage phenotype in costochondral cells. *Arthritis Research & Therapy*, 15(6), R214 https://doi.org/10.1186/ar4409.

Murphy, M. K., Huey, D. J., Reimer, A. J., Hu, J. C., & Athanasiou, K. A. (2013). Enhancing post-expansion chondrogenic potential of costochondral cells in self-assembled neocartilage. *PLoS One*, 8(2), e56983. https://doi.org/10.1371/journal.pone.0056983.

Murphy, M. K., Masters, T. E., Hu, J. C., & Athanasiou, K. A. (2013). Engineering a fibrocartilage spectrum through modulation of aggregate redifferentiation. *Cell Transplantation*, https://doi.org/10.3727/096368913X676204.

Neu, C. P., Khalafi, A., Komvopoulos, K., Schmid, T. M., & Reddi, A. H. (2007). Mechanotransduction of bovine articular cartilage superficial zone protein by transforming growth factor beta signaling. *Arthritis and Rheumatism*, 56(11), 3706–3714 https://doi.org/10.1002/art.23024.

O'Sullivan, N. A., Kobayashi, S., Ranka, M. P., Zaleski, K. L., Yaremchuk, M. J., Bonassar, L. J., & Randolph, M. A. (2015). Adhesion and integration of

tissue engineered cartilage to porous polyethylene for composite ear reconstruction. *Journal of Biomedical Materials Research. Part B, Applied Biomaterials*, *103*(5), 983–991 https://doi.org/10.1002/jbm.b.33269.

Peng, G., McNary, S. M., Athanasiou, K. A., & Reddi, A. H. (2015). The distribution of superficial zone protein (SZP)/lubricin/PRG4 and boundary mode frictional properties of the bovine diarthrodial joint. *Journal of Biomechanics*, *48*(12), 3406–3412 https://doi.org/10.1016/j.jbiomech.2015.05.032.

Proffen, B. L., McElfresh, M., Fleming, B. C., & Murray, M. M. (2012). A comparative anatomical study of the human knee and six animal species. *The Knee*, *19*(4), 493–499 https://doi.org/10.1016/j.knee.2011.07.005.

Shiomi, T., Nishii, T., Nakata, K., Tamura, S., Tanaka, H., Yamazaki, Y., ... Sugano, N. (2013). Three-dimensional topographical variation of femoral cartilage T2 in healthy volunteer knees. *Skeletal Radiology*, *42*(3), 363–370 https://doi.org/10.1007/s00256-012-1522-2.

Stacey, M., Dutta, D., Cao, W., Asmar, A., Elsayed-Ali, H., Kelly, R. Jr., & Beskok, A. (2013). Atomic force microscopy characterization of collagen 'nanostraws' in human costal cartilage. *Micron*, *44*, 483–487 https://doi.org/10.1016/j.micron.2012.10.006.

Stacey, M. W., Grubbs, J., Asmar, A., Pryor, J., Elsayed-Ali, H., Cao, W., ... Kelly, R. E. Jr. (2012). Decorin expression, straw-like structure, and differentiation of human costal cartilage. *Connective Tissue Research*, *53*(5), 415–421 https://doi.org/10.3109/03008207.2012.684113.

Xingzhou, Q., Chenping, Z., Laiping, Z., Min, R., Shanghui, Z., & Mingyi, W. (2011). Deep circumflex iliac artery flap combined with a costochondral graft for mandibular reconstruction. *The British Journal of Oral & Maxillofacial Surgery*, *49*(8), 597–601 https://doi.org/10.1016/j.bjoms.2010.10.008.

Yazdanbakhsh, A. P., van Rijssen, L. B., Koolbergen, D. R., Konig, A., de Mol, B. A., & Hazekamp, M. G. (2015). Long-term follow-up of tracheoplasty using autologous pericardial patch and strips of costal cartilage. *European Journal of Cardio-Thoracic Surgery*, *47*(1), 146–152 discussion 152. https://doi.org/10.1093/ejcts/ezu101.